*Journal of Thermal Analysis and Calorimetry, Vol. 71 (2003) 951–966*

# IDENTIFICATION OF MICRO-SCALE CALORIMETRIC DEVICES
# IV. Descriptive models in 3-D

*C. Auguet*[1], *J. Lerchner*[2], *P. Marinelli*[3], *F. Martorell*[1], *M. Rodriguez de Rivera*[4], *V. Torra*[1*] *and G. Wolf*[2]

[1]CIRG-DFA-ETSECCPB, Polytechnical University of Catalonia, Campus Nord B-4, E-08034 Barcelona, Spain
[2]Institut f. Physikalische Chemie, TU Bergakademie Freiberg, Leipziguer Str. 29, D-09596 Freiberg/Sachsen, Germany
[3]Centro Atomico Bariloche and Instituto Balseiro, 8400 San Carlos de Bariloche, Argentina
[4]Physics Dept. ETSII. Las Palmas University, Campus of Tafira (Basic Science Building), E-35017 Las Palmas de Gran Canaria, Spain

## Abstract

The experimental analysis of conventional conduction calorimeters shows excellent reproducibility and relevant systematic errors in comparison with thermodynamic values established via adiabatic calorimeters. Two examples: a DSC and a liquid flow device are schematically analyzed. When an increased accuracy will be obtained the positional effects on the experimental set-up and on the measurement process need to be modelled. From experimental measurements realized on the Xensor liquid nano-calorimeter representative models can be built. To evaluate the reliability of measurement routines, established from experimental basis, several different dissipation structures inside the working space can be simulated. Two experimental configurations related to drop to drop reaction and to continuous mixing are modelled via RC approach. The RC formalism is extended to evaluate the carried energy effect produced by the continuous inflow/outflow of reactants in the mixing enthalpy chamber.

**Keywords:** accuracy, conduction calorimeter, Fourier equation, heat and mass transfer, mixing enthalpy, models, simulation

## Introduction

The actual applications of isothermal conduction calorimeters [1, 2] and of temperature programmed devices as ATD or DSC requires an improved sensitivity to compensate the extremely reduced mass of the samples. The miniaturization process is fuelled by the technological needs to reduce the quantity of new synthesized and expensive substances. Manufactured by Xensor, the liquid nano-calorimeter is one of

* Author for correspondence: E-mail: vtorra@fa.upc.es

*1388–6150/2003/ $ 20.00*
*Akadémiai Kiadó, Budapest*

the available sensors on the market [3]. When an appropriate box is built, the device operates as a non-differential calorimeter in, for instance, isothermal conditions. Appropriate covers and auxiliary equipment permits several microdevices for analytical characterization. The working surface (as a nose detector of gas mixture [4]) is close to 15 $mm^2$. The working volume is situated under 20 μL in integral enthalpy measurements, i.e. via drop to drop mixture [5] or via continuous mixing [6].

The volume reduction and the thin film deposition methods in flat surfaces induce auxiliary problems related to heat flux detector. The main problem, a common problem in the available devices, relates the heat flux integration: From the 4π stereo-radians surrounding the sample or 'reacting volume', the surface covered by the detector is practically zero [7, 8]. The device furnishes reproducible results but the extremely lower detected surface is the origin of inaccurate results. In fact, the device works mainly as a sensitive sensor not as an integrating heat-flux-meter. This particular situation suggests that improved formalisms need to be developed. In general, the use of specific thin films as detectors in host-guest reactions is a common method using, for instance, resistance or electrical measurements [9–11] but the quantitative difficulties are a subject of permanent interest.

The general target of this series of connected papers entitled 'Identification of micro-scale calorimetric devices' relates the search of justified experimental approach to increased accuracy in conduction calorimeters and in programmed temperature devices**. In the paper I, the positional effects in a classical DSC device are visualized, an experimental approach to the free Xensor device is outlined and the shape factor is introduced [7, 8]. In paper II a 2-D model, describing the experimental behavior, is built [12]. In paper III [13], the 3-D device is experimentally analyzed, the rate effects studied and practical rules to determine the enthalpy results are proposed.

The main content of this paper is twofold. In the first one, a partial analysis centered on standard manufactured device shows that the Xensor micro-devices behavior is similar. For it, in a DSC with detection situated in bottom flat surface of the crucible, the *z*-coordinate effect is visualized. Also, by means of a set-up devoted to the liquid mixtures, the dependence response with the volume rate and the type of liquid is displayed. In the second one, centered on modelling, two RC models [1, 14–20] corresponding to the Xensor devices and related to mixing enthalpy evaluation are built. The practical target of a representative model relates the simulation of different 3-D dissipation in the available 'reaction' volume: i.e. the *z*-effects, the 3-D dissipation and the volume rate actions. The preliminary values of the parameters characterizing the heat transfer model are optimized using a classical Marquardt approach [12, 21, 22]. The model permits an evaluation of Shape Factor effects and/or of the geometric actions related to the dissipation position. A roughly generalization permits the inclusion of the energy transfer induced by mass flows in the heat transfer formalism.

** A cooperative research program is established between the authors to analyze the behavior of flat detectors (in particular, the Xensor device) via experimental measurements and appropriate simulation. The main target relates an accuracy improvement in energy measurement traceable to Joule dissipation. Subsequently, practical rules modifying the sensitivity value of the manufacturer heater will be established.

## Classical effects on conventional devices

The difference among the thermodynamic values and the energy measured in conduction calorimeters in the old [23] and in actualized counterparts [24] is a classic problem that requires permanent attention. For instance, some of the difficulties that present two conventional measurement systems are visualized. They are based on the detection of the heating flow that is exchanged between the 'reaction' area (i.e. the crucible or the reaction chamber) and the surroundings. Two types of classical devices are used with particular effects in the energy measurements. The first one, a standard DSC device (TA Instrument 2910 MDSC V4.3 B) (Fig. 1) usually destined to measure the latent heat in first order phase transition, to analyze the glassy transitions and to determine the temperature effects on the specific heat. The device shows remarkable effects with the distance between the detectors and the heater: in a solid–solid phase transformation (some effects related to martensitic transformation are presented in reference 7) or in Joule effect in a resistance (Fig. 2). In other words, the sample thickness plays a relevant effect on the energy measurements: more sophisticated calibration process is necessary when more quantitative results are required. In particular, in phenomena with distributed energy dissipation 'different' of the standard phenomena (as, for instance, In melting) used in calibration procedures. The second one, a liquid flow calorimeter (flow isotherm microcalorimeter TAM 2277-204 by Thermometric AB) working in isothermal conditions shows changes in sensitivity related to volume rate and liquid type (Fig. 3). The two examples are representative of the flat detector systems: there is a relevant dependence with the distance to the detector, with the thermal properties of the material and, in the case of systems of continuous flow, with the flow rates.

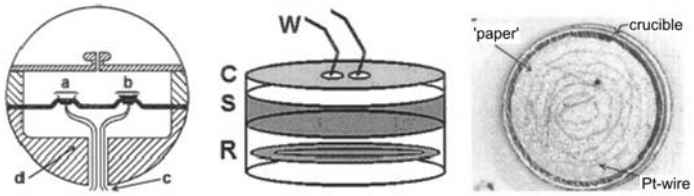


**Fig. 1** Left: outline of the standard DSC device (TA Instrument 2910 MDSC V4.3 B); a – reference crucible; b – sample crucible; c – thermocouple wires; d – programmed temperature block. Center: schematic structure of used crucibles in Joule measurements. Two types of heaters are prepared: with the Pt-wire in the bottom (lower *z*-distance) and in the top of the crucible (higher *z*-distance). W: wires for Joule pulses; C: crucible covered by an Al foil; S: epoxy shell; R: Pt-resistance wire and cellulose isolation. Right: photograph of the resistance preparation in the crucible bottom. 'Paper': two sides of gummed cellulose shell

In DSC device (Fig. 1) two standard Al crucibles are modified. Inside the crucible, a Pt-resistance is embedded inside a cellulose shell and situated under (resistance 'bottom') or over a shell of epoxy (resistance 'top'). Series of Joule pulses (using 352

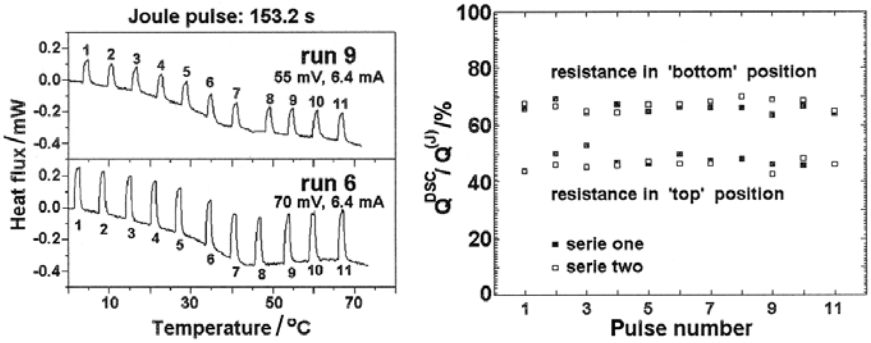


**Fig. 2** Left: series of calorimetric signals related to two different dissipated Joule powers in the crucibles. Right: changes induced by the heater position (*z*-coordinate effect) via four independent series of measurements: mounting and dismounting and using different crucibles

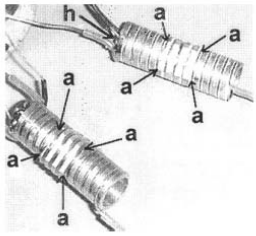


**Fig. 3** Cell support and spiral tube in the differential 'flow isotherm microcalorimeter TAM 2277-204 (Thermometric AB)'. h – position of the manufacturer's heater; arrows a – situation of the detector by a semiconductor thermocouple plate

and 448 μW) are dissipated in each crucible. Always the used temperature rate is 0.5 K $min^{-1}$ and the temperature domain is situated between –10 and 80°C. The position effect is determined dividing the energy measured (the device is calibrated via the classical In melting) by the furnished Joule effect. Some dispersion is observed for different runs and complete repositioning of the crucibles (under 5%). High relevant differences are related with the *z*-position of the heater Pt-resistance (Fig. 2 right). Homogeneous dissipation in low conducting materials (Fig. 2) suggests a mean difference close to 30% (similar to absolute differences observed in [23]).

The calorimeter (flow isotherm microcalorimeter TAM 2277-204 Thermometric AB) is designed to determine the mixing enthalpy from the output signal in steady state: The 'reaction' dissipates constant power. For instance the molar mixing enthalpy, associated to constant flow rates of the pure liquid components, produces a constant calorimetric signal in steady state. The absorbed heat power $W_{absorb}$, related with the thermodynamic enthalpy change ($\Delta H^M$) and the molar rate of the two components (A and B), could be represented by,

$$W_{\text{absorb}} = \Delta H^{\text{M}} \dot{n} = \Delta H^{\text{M}} \left( \frac{\mathrm{d}n_{\text{A}}}{\mathrm{d}t} + \frac{\mathrm{d}n_{\text{B}}}{\mathrm{d}t} \right) \quad (1)$$

The device also permits the evaluation of the excess molar partial enthalpies and/or of the apparent relative molar enthalpies. For instance, via dissolution or dilution processes respectively. In these measurements, the liquid accumulates in the cell so that their contents grow progressively. The steady state measurement method requires a continuous flow of the two components. In the device, the mixture is carried inside the tube twisted around the cell. The detector (a semiconductor thermocouple plate) is located in the central part of the spiral pipe. See the squared zone indicated by the arrows *a* in Fig. 3.

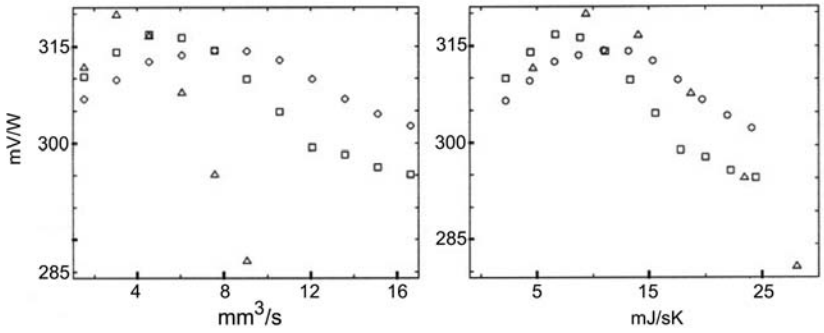


**Fig. 4** Left: flow volume rate effects on sensitivity (mV/W) for three mixtures using the $\Delta H^{\text{M}}$ from the literature values: □ – benzene+cyclohexane [28]; o – cyclohexane+hexane [29]; △ – water+methanol [30]. Right: sensitivity (mV/W) *vs*. the heat capacity rate (d*C*/d*t*) for the same mixtures

The sensitivity in flow calorimeters depends on diverse factors [25–27]. In the first place, the effect produced by the volume rate. The position of the detector induces an increase of the sensitivity as the flow rate increases and the mixture is carried out more close to detector. Increasing flow rate, the sensitivity arrives to a maximum and, after, decreases progressively: a part of the components doesn't have time to react inside the tube close to the detection area. Also, the flow transports some unmeasured energy directly to the external surroundings. The representation in function of the heat capacity rate provides a more reduced dispersion. The similar behavior of the experimental data shows the especial relevance of the d*C*/d*t* value. Other parameters (viscosity or effects of the interface energy) maintain some differences for each substance. The signal to noise ratio in measurements given in Fig. 4 is relatively lower situated between 40 to 320 (i.e., between 32 to 50 in dB scale).

## Experimental devices and symmetry constrains

The experimental devices studying the drop to drop 'reaction' and the mixing enthalpy via continuous mixing are outlined in Fig. 5. Both systems, based on the

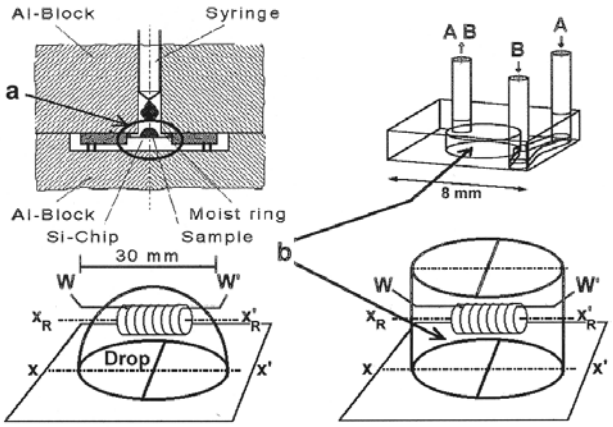


**Fig. 5** Schematic representation of devices based on Xensor Liquid nano-calorimeter LCM 2524. In the outlined configuration each set-up works in 'static' situation heated by resistance and a quarter can represent the system. Left: drop to drop reaction. Bottom left: drop with a Pt-resistance (spring shape) with squared symmetry (enlarged from a). Right: example of chamber for continuous flow mixtures. A and B: inlets; AB: outlet. Bottom right: the cylindrical shape of the liquid chamber, the squared shape of the plastic chamber and of the Xensor device and the spring shape of Pt-resistance establishes a global squared symmetry in Joule measurements. W, W': electrical wires

Xensor chip, are described elsewhere [5–10]. Several Pt-resistance in different positions, liquid contents and volume rates (in chamber analysis) determines the experimental output signal *vs*. time or DSC curve related to each configuration [10] corresponding to a well determined input (i.e. a Joule step or Heaviside signal).

The chamber, associated to continuous mixture, is square shaped as the Xensor free detector. The liquid volume has cylindrical symmetry. The Joule study is realized mainly via straight coils in Pt wire (diameter 0.8 mm). Indeed, the complete system has squared symmetry: a quarter is sufficient to describe the complete 'Joule' behavior. As a first approach, a cylindrical sector also shows the main sensitivity characteristics: the radial and the *z*-axis effects. In true measurements (mixing enthalpy studied by liquid flows) the quaternary symmetry is broken and a more complete model is necessary. When the liquids are introduced simultaneously via, for instance, the T-shaped system [13] or an inlet of coaxial tubes, the representation needs at least a half of the device: a mirror symmetry, induced by the privileged axis imposed by the inlet-outlet plane, can be used. The simplified geometry of drop to drop reactions suggests the use of cylindrical symmetry or, for more detailed actions in Joule measurements, the representation by a quarter of the system.

## The Fourier approach: RC models in the 3-D configurations

The decomposition of a 3-D system in $N$ finite domains each one at uniform temperature $T_j$, with $C_j$ heat capacities and $P_{jk}$ thermal couplings between elements and $P_j$ to

external surrounding temperature $T_0$, permits a classical treatment. The instantaneous energy balance furnishes a system of linear differential equations:

$$W_j = C_j \frac{dT_j}{dt} + \sum_{k \neq j} P_{jk}(T_j - T_k) + P_j(T_j - T_0); \quad j=1, 2, ..., N \tag{2}$$

For an experimental device with thermopairs, the experimental output (or DSC curve) can be represented by a sum of temperature differences (one for each pair). Each output (or DSC curve), related to a particular dissipation distribution in $l$ elements (with $l$–$N$), implies the appropriate convolution as is described elsewhere [15–20]. In the calorimetric output are included: the $l$ dissipation positions in the domains $k_1^*, k_2^*, ...k_1^*$ and the $n$ thermopairs $(m_1^*, m_2^*, ...m_n^*)$ each one in two temperature domains corresponding to warm and to cold junctions. The DSC curve is represented by a sum of convolutions (in time coordinate) or a sum of products in Laplace coordinated by:

$$\begin{aligned} s(t) &= s(t, W_{k_1^*}, W_{k_2^*}, ..., W_{k_1^*}, m_1^*, m_2^*, ..., m_n^*) = \\ &= \pounds^{-1}\left[\sum_{k^*=k_1^*}^{k^*=k_1^*} W_{k^*} TF_{k^*}(p, m_1^*, m_2^* ..... m_n^*)\right] \end{aligned} \tag{3}$$

The operator $\pounds^{-1}$ is the inverse Laplace transform: shifts from the Laplace coordinate $p$ to the time coordinate $t$. In Laplace coordinate, the $W_{k^*}(p)$ relates the dissipated power in one of the $k^*$ elements and the $TF_{k^*}$ (for all detectors) reads,

$$TF_{k^*}(p, m_1^*, m_2^*, ...m_n^*) = k_{Seebeck} \sum_{m^*=m_1^*}^{m^*=m_n^*} [T_{m^*(warm)}^{\delta(t) \text{ in } k^*}(p) - T_{m^*(cold)}^{\delta(t) \text{ in } k^*}(p)] \tag{4}$$

The $k_{Seebeck}$ coefficient converts the temperature units to an output voltage (i.e. from K to V). The $T_{m^*(warm)}^{\delta(t) \text{ in } k^*}(p)$ and the $T_{m^*(cold)}^{\delta(t) \text{ in } k^*}(p)$ are, respectively, the 'temperature' (in Laplace coordinate units: K s) in the warm and in the cold junctions for each thermocouple $m^*$ associated to a heat power pulse ($\delta(t)$ a Dirac signal of 1 J) only dissipated in each $k^*$ position. The equations are coherent with the experimental reality: a universal transfer function doesn't exist: the dissipation is not produced in only one point of the crucible. In the linear domain of the system, each position of the dissipation contributes independently. The formalism allows the influences that produce each dissipation element on the total output: each dissipating element contributes with a particular transfer function that relates the dissipation place with the detector system. Usually, the detector system is an invariant of the experimental set-up. The model can be numerically solved via software packages of linear systems. Dividing by $C_j$, the temperature derivatived reads,

$$\frac{dT_j}{dt} = \frac{W_j}{C_j} - \left(\sum_{k \neq j} \frac{P_{jk}}{C_j}(T_j - T_k) + \frac{P_j}{C_j}(T_j - T_0)\right); \quad j=1,2..., N \tag{5}$$

Using $T_0$ as the temperature reference, the previous equation can expand to:

$$\frac{\mathrm{d}T_\mathrm{j}}{\mathrm{d}t}=\frac{W_\mathrm{j}}{C_\mathrm{j}}+\frac{P_\mathrm{j1}}{C_\mathrm{j}}T_1+\frac{P_\mathrm{j2}}{C_\mathrm{j}}T_2+\ldots-\left(\frac{P_\mathrm{j}}{C_\mathrm{j}}+\sum_{\mathrm{k}\neq\mathrm{j}}\frac{P_\mathrm{jk}}{C_\mathrm{j}}\right)T_\mathrm{j}+\ldots+\frac{P_\mathrm{jN-1}}{C_\mathrm{j}}T_\mathrm{N-1}+\frac{P_\mathrm{jN}}{C_\mathrm{j}}T_\mathrm{N};\ j=1,\ldots,N \quad (6)$$

Defining the vectors $T$, $\mathrm{d}T/\mathrm{d}t$ and $B$ and the matrix $A$ by:

$$T=\begin{pmatrix}T_1\\T_2\\\ldots\\T_\mathrm{N}\end{pmatrix};\quad \frac{dT}{dt}=\begin{pmatrix}\frac{\mathrm{d}T_1}{\mathrm{d}t}\\\frac{\mathrm{d}T_2}{\mathrm{d}t}\\\ldots\\\frac{\mathrm{d}T_\mathrm{N}}{\mathrm{d}t}\end{pmatrix};\quad B=\begin{pmatrix}\frac{W_1}{C_1}\\\frac{W_2}{C_2}\\\ldots\\\frac{W_\mathrm{N}}{C_\mathrm{N}}\end{pmatrix}$$

$$A=\begin{pmatrix}-\left(\frac{P_1}{C_1}+\sum_{\mathrm{k}\neq1}\frac{P_\mathrm{1k}}{C_1}\right) & \frac{P_{12}}{C_1} & \ldots & \frac{P_\mathrm{1N}}{C_1}\\\frac{P_{21}}{C_2} & -\left(\frac{P_2}{C_2}+\sum_{\mathrm{k}\neq2}\frac{P_\mathrm{2k}}{C_2}\right) & \ldots & \frac{P_\mathrm{2N}}{C_2}\\\ldots & \ldots & \ldots & \ldots\\\frac{P_\mathrm{N1}}{C_\mathrm{N}} & \frac{P_\mathrm{N2}}{C_\mathrm{N}} & \ldots & -\left(\frac{P_\mathrm{N}}{C_\mathrm{N}}+\sum_{\mathrm{k}\neq\mathrm{N}}\frac{P_\mathrm{Nk}}{C_\mathrm{N}}\right)\end{pmatrix} \quad (7)$$

The formalism can be written with the state vector structure as:

$$\frac{\mathrm{d}T}{\mathrm{d}t}=A\,T+B \quad (8)$$

Standard numerical methods as, for instance, Matlab with appropriate linear toolbox, agree very well with the state vector representation. From the calculated $T_{\mathrm{m}^*}(t)$ using the complete set of dissipated power $W_{\mathrm{k}_1^*},W_{\mathrm{k}_2^*},\ldots W_{\mathrm{k}_\mathrm{l}^*}$ the sum of temperature differences (warm and cold junctions) furnishes the simulated output signal by,

$$s(t)=k_\mathrm{Seebeck}\sum_{\mathrm{m}^*=\mathrm{m}_\mathrm{l}^*}^{\mathrm{m}^*=\mathrm{m}_\mathrm{n}^*}\left(T^{W_{\mathrm{k}_1^*,\ldots,\mathrm{k}_\mathrm{l}^*}}_{\mathrm{m}^*\,(\mathrm{warm})}(t)-T^{W_{\mathrm{k}_1^*,\ldots,\mathrm{k}_\mathrm{l}^*}}_{\mathrm{m}^*\,(\mathrm{cold})}(t)\right) \quad (9)$$

The two formalisms, solving via the TF and the appropriate convolutions (F in Table 1) or, directly, via the state vectors (ML in Table 1), are completely equivalent. Using a model with high number of elements, the numerical constraints related to truncation and error propagation can produce similar pattern (Table 1) but, also, a little bit different results (observed differences under 5%).

**Table 1** Sensitivity values in relative scale (reference: chip heater and ethanol) calculated and experimental for each available heater: chip heater and Pt-resistance in bottom, medium or top position. Homogeneous: calculated value when a homogeneous dissipation is produced inside the chamber. F: estimated using transfer function and convolution. ML: calculated by state vectors

| Chamber contents | Chip heater | R: bottom | R: medium | R: top | Homogeneous |
|---|---|---|---|---|---|
| EtOH (experimental | 1.000 | 0.788 | 0.677 | 0.562 | – |
| EtOH (calculated F) | 1.000 | 0.823 | 0.717 | 0.673 | 0.771 |
| EtOH (calculated ML) | 1.000 | 0.814 | 0.669 | 0.609 | 0.743 |
| $H_2O$ (experimental) | 0.949 | 0.791 | 0.752 | 0.670 | – |
| $H_2O$ (calculated F) | 0.980 | 0.823 | 0.748 | 0.719 | 0.785 |
| $H_2O$ (calculated ML) | 0.975 | 0.857 | 0.785 | 0.757 | 0.821 |

*Symmetries: the tool for complexity reduction*

The symmetry permits more sophisticated treatment with minor number of elements. Using N elements is possible to build a model similar to the 3-D structure as, for instance, a drop on the Xensor working chip surface. In the drop surface heat losses to surroundings need to be introduced and, obviously, the sensitivity (or detected signal) is related to the heat fraction between the detected heat *vs.* the heat lost [7]. This ratio depends on the relative position of the dissipated heat: more close to warm junctions or more close to the external surroundings [7, 31]. The situation is similar for the flow device. In static configuration, the chip, the cover and the heater can be modelled by only one quarter of the complete device. See, in Figs 6 and 7 the element distribution in drop ($N$=38 in shells $D$, $C_b$, $C_m$ and $C_t$) and in flow chamber ($N$=56 in shells $E$, $D$, $C_b$, $C_m$ and $C_t$).

The model needs the creating the network of the elements and, subsequently, the determination of the heat capacities and thermal couplings with the neighbour elements. For instance, in the angular sector ($\alpha$) of thickness $h$ represented in Fig. 8 three

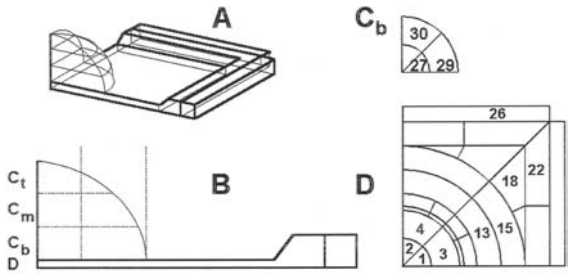


**Fig. 6** Outline of the RC models ($N$=38). A: one quarter of the drop scheme (drop and chip working surface); B: front view with one of the vertical grid shells of drop ($C_t$, $C_m$, and $C_b$) and $D$ (silicon working surface and rim). Right: associated numbers of the simulated heat capacities

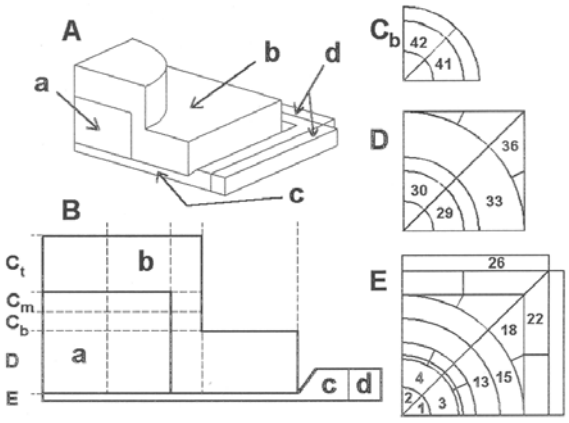


**Fig. 7** Outline of the RC models. A: chamber for continuous mixing (a quarter). a – liquid contents; b – chamber in Plexiglas; c – silicon working surface and rim; d – connection to chip device protection package; B: front view with one of the vertical grid shells ($C_t$, $C_m$, $C_b$, $D$ and $E$ with 56 elements). Right: allocation of heat capacities reference numbers in level $C_b$, $D$ and $E$

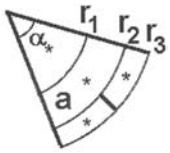


**Fig. 8** Outline of network established in a sector of α radians with thickness $h$. * – center of the elements; a – used element for thermal resistance evaluation (see, text)

thermal resistance (inverse of the heat loses coefficient P) are searched: in radial, in axial and in $z$-direction. For each element the center of symmetry is estimated and each thermal resistance is evaluated between the centers of neighbour elements. For instance, the three thermal resistance values associated to the complete '*a*' element (between the opposite surfaces) in radial, in axial (for lower α values) and in the $z$-axis direction read,

$$R_{\text{radial}} = \int_{r=r_1}^{r=r_2} \frac{\mathrm{d}r}{k\alpha r h} = \frac{1}{k\alpha h} \ln\left(\frac{r_2}{r_1}\right);\ R_{\text{axial}} = \frac{\alpha (r_2 + r_1)/2}{kh(r_2 - r_1)};\ R_{\text{z-coord.}} = \frac{h}{k\alpha (r_2^2 - r_1^2)} \qquad (10)$$

Starting from the network, each volume furnishes the heat capacity and the geometric characteristics allow determining the values of the thermal couplings. The used basic data have been obtained of [28]. Once basic model is built, it is possible to carry out adaptations and improvements. The chamber system can be reorganized with two shells of type $D$ and only two of the type $C$. Using this last possibility the liquid is distributed in three vertical more homogeneous layers $E$, $D_b$, $D_t$, $C_b$ and $C_t$ ($N$=62).

The representative model for the chamber increases their complexity when the symmetry decreases to mirror symmetry or, eventually, to describe the complete device. For instance, when an actual mixture process will be simulated.

## Comparison between experimental and simulated results

Starting from the model outlined in Fig. 7 and of the values of the thermal properties of the Table 2 the output signals (DSC curves) related to a Heaviside step have been calculated. From the DSC curve the sensitivities are evaluated and compared with the experimental observations (Table 1). Also, the behavior of two different liquids has been simulated (ethanol and water) inside the working chamber (Fig. 9). The qualitative behavior of the model is coherent with the experimental curves. In particular, the model permits a prediction of the sensitivity for any dissipation configuration. In the Table 1, the relative sensitivity has been calculated when a homogeneous power is dissipated in the complete liquid volume. The simulation allows the evaluation of the shape factor. It is necessary to divide the calculated sensitivity when the dissipation is carried out with the space distribution of interest for the calculated value obtained dissipating in the chip heater.

*Ethanol and water after a Marquardt fit*

To obtain an approach to the behavior that visualizes the dynamic effects of the mass flow, the parameters of the 'static' system are optimized by means of the Marquardt method [33] and the experimental observations corresponding to the ethanol and water have been used. The methodological approach is described in the paper II [12][***]. The Fig. 9 shows a satisfactory coherence between the ethanol and water measurements and each particular fit: the thermal parameters of the device box need to be fitted to each fluid.

## From static models to rate effects simulations: Extended RC models including the energy flow carried by mass transfer

The liquid flow transports energy. Each volume element used for the RC description is influenced by the permanent exchange of mass (Fig. 10). In the time interval d$t$ there are an input and output of mass with the neighbouring elements: an energy exchange not included in the RC formalism. Two working hypothesis permit a roughly approach:

*** The approach to physical parameters ([12] describing the two-dimensional device and for general information [33]) is realized via fitting of experimental data: an adapted Marquardt method has been used. The method (a non-linear fit), estimates the dependence of the squared error (difference between experimental and calculated points) with each researched parameter ($a_i$). The $a_i$ represents 'free' parameters to be fitted: i.e. the heat capacities, the thermal couplings, the heat losses, the time delay, and so on.

**Table 2** Thermal properties for the materials [32] involved in the simulation

| Property | Material | | | | | |
|---|---|---|---|---|---|---|
| | Silicon | Water | Ethanol | Glycerol | Plexiglas | Gum |
| Thermal conductivity/ W $m^{-1}$ $K^{-1}$ | 148 | 0.6076 | 0.180 | 0.286 | 0.26 | 0.249 |
| Heat capacity/J $kg^{-1}$ $K^{-1}$ | 2.33d+03 | 1.0d+03 | 2.38d+03 | 2.39d+03 | 1.41d+03 | 2.382d+03 |
| Density/kg $m^{-3}$ | 0.705d+03 | 4.186d+03 | 0.789d+03 | 1.204d+03 | 1.448d+03 | 1.116d+03 |

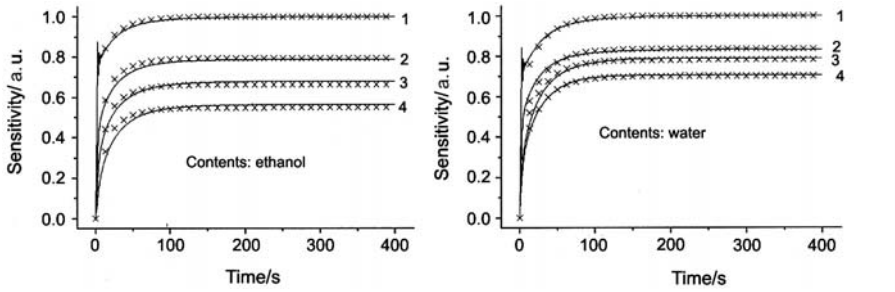


**Fig. 9** Output signals (experimental and calculated DSC curves) *vs*. time for different heaters relative to chip heater sensitivity: — – experimental and x – calculated. Chamber contents: ethanol (left) and water (right). 1 – chip resistance; 2 – heater in bottom position; 3 – heater in medium position; 4 – heater in top position. Some filtering ripple appears in the fast part of the experimental chip heater signals

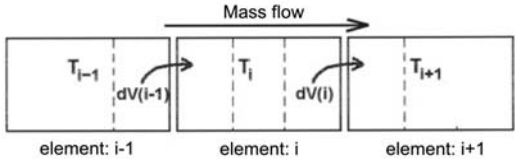


**Fig. 10** Schematic outline of the mass (or volume) transfer in the element *i*. In the time d*t* the same volume d*V* enters in the *i*-element from the element *i*–1 (at $T_{i-1}$) and, also, it is transferred to the element *i*+1 at temperature $T_i$

1) The volume from the element *i*–1 acquires the temperature of the element *i*. With this hypothesis it is not necessary to consider that the energy is transferred to the next element.

2) The energy transfer can be represented by a Newtonian term. The net heat power ($W_{i-1\to i}$) given by the liquid flow transferred from the *i*–1 element (at $T_{i-1}$) to the *i* element (at $T_i$) can be represented by:

$$W_{i-1\to i}=k\rho\frac{dV}{dt}c(T_{i-1}-T_i)=kP^*_{i-1,i}(T_{i-1}-T_i) \tag{11}$$

The inflow of the liquid volume (d*V*/d*t* from the *i*–1 to the *i* element) induces a net input of energy in the element *i* related to the temperature difference between the actual element (*i*) and the previous element (*i*–1) [21, 26]. The appropriate auxiliary and non-symmetrical couplings ($P^*_{i-1,i}$) permits a qualitative visualization of the volume rate effects. At reduced values of flow rates, the adapted formalism can be solved as the RC analogy. The actual simulation uses a rough approach: only a quarter of the device. More reasonable flow simulation needs, at least, a half of the device. The *k* parameter ($k\in[0, 1]$) represents the effective percent of the transferred energy via the mass flow. Figure 11 shows the qualitative evolution of the simulated sensitivity *vs*. the volume rate. A preliminary comparison between calculated values and

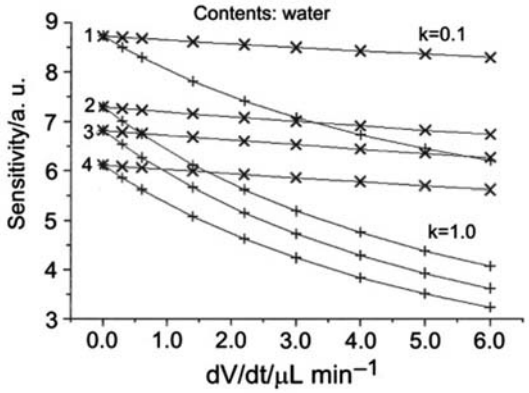


**Fig. 11** Sensitivity changes *vs.* the volume rates (simulation), related to resistance position and to $k$ values. 1 – chip heater; 2 – resistance situated in the bottom of the chamber; 3 – situated in the middle of the chamber; 4 – heater on the upper part of the chamber. + – $k$ =1.0; x – $k$ =0.1

experimental measurements (for instance, Fig. 7 in [13]) suggest that the $k$ value do not overcome 0.40. The actual rough observations suggest that part of the mass travels without heat transfer and, in coherence with flow devices (Fig. 4), without sufficient time for appropriate mixing.

## Conclusions

The positional effects ($z$-dependence) in conventional DSC devices are extremely important with lower thermal conductivity contents. Differences between measured and dissipated energy, up to 30 to 50% and dependent of crucible contents, can be observed. The effects of volume rate in standard flow isotherm microcalorimeter are included inside an uncertainty close to ±4%.

Several complex RC-models can be built to describe the 3-D working systems (in static behavior) used in Xensor devices: drop to drop and continuous flow mixtures. The response of the models shows the main particularities of the experimental devices: squared (or radial) symmetry dependence and big $z$-effect if the heater (or the internal dissipation) is separated from the silicon surface. Eventually, the model can be fitted for a better match with experimental measurements using the standard Marquardt approach. From the model is possible to evaluate the shape factor for each heating type configuration.

In flow measurements the heat and mass transfer induces relevant effects in the system not included in the classical heat transfer equations. For instance, the energy dissipated in the reaction can be directly transferred to the outlet: The RC models are extended to include the relevant heat transfer effects related with the mass-flow. In the actual level of the formalism the analysis does not include the effects related to the true advancement

of the reaction, i.e. related to the particularities of the reactants and to the actions induced by the low mixing between two 'laminar flow' of reactants.

* * *

The work is carried out in the frame of cooperative program (Barcelona, Las Palmas, Freiberg, Bariloche and Marseilles) centered on the accuracy of conduction calorimeters and derived devices. The cooperation is supported via integrated HA 1999-0087 (MCT-Spain) and 314-Al-e-dr (DAAD, Germany) ACI-99 2 and 6 (Gen. of Catalonia). The ACES 1999-00040 (Gen. of Catalonia) related to 'nanocalorimeters' is gratefully acknowledged. The stay of F. M. in TU Bergakademie Freiberg is realized in the frame of SOCRATES program. Part of this work was further founded by the German Research Council (Deutsche Forschungsgemeinschaft) under grant Wo 576/5-3.

## References

1 A. Tian, Recherches sur la Calorimétrie par compensation. Emploi des effets Peltier et Joule. Étude d'un microcalorimètre intégrateur, oscillographe et ballistique, Louis Jean, Imprimeur, Gap, 1931.
2 E. Calvet and H. Prat, Microcalorimétrie, Masson 1956.
3 Xensor, Liquid nanocalorimeter by Xensor Integration, Delft, The Netherlands, (website: www.xensor.nl).
4 J. Lerchner, D. Caspary and G. Wolf, Sensors and Actuators B, 70 (2000) 57.
5 J. Lerchner, A. Wolf and G. Wolf, J. Therm. Anal. Cal., 57 (1999) 241.
6 A. Wolf, A. Weber, R. Hüttl, J. Lerchner and G. Wolf, Thermochim. Acta, 337 (1999) 27.
7 V. Torra, C. Auguet, H. Tachoire, P. Marinelli and J. Lerchner, J. Therm. Anal. Cal., 66 (2001) 255.
8 J. Lerchner, G. Wolf, C. Auguet and V. Torra, Thermochim. Acta, 382 (2002) 65; Thermochim. Acta, 382 Issue 1-2, 31 January 2002, Developments in Calorimetry 2001, Freiberg, Germany, 21 March 2001, Ed. W. Hemminger, G. W. H. Hohne and G. Wolf.
9 P. Lauque, M. Bendahan, C. Jacolin, J. L. Seguin, M. Pasquinelli and P. Knauth, 'Electrical properties and sensor characteristics for $NH_3$ gas of sputtered CuBr thin films', Sensors and Actuators B, 59 (1999) 216.
10 P. Lauque, M. Bendahan, J. L. Seguin, M. Pasquinelli and P. Knauth, Solid State Ionics, 136–137 (2000) 603.
11 M. Bendahan, C. Jacolin, P. Lauque, J. L. Seguin and P. Knauth, J. Phys. Chem., B, 105 (2001) 8327.
12 C. Auguet, F. Martorell, F. Moll and V. Torra, J. Therm. Anal. Cal., 70 (2002) 277.
13 C. Auguet, J. Lerchner, V. Torra and G. Wolf, J. Therm. Anal. Cal., to be published.
14 S. C. Mraw, Rev. Sci. Instrum., 53 (1982) 228.
15 G. Hohne, W. Hemminger and H.-J. Flammersheim, Differential Scanning Calorimetry, Springer, Heidelberg 1996.
16 J. L. Macqueron, J. Navarro and V. Torra, An. Fis., 73 (1977) 163.
17 E. Cesari, J. Hatt, E. Margas, J. Navarro, V. Torra, E. Utzig and W. Zielenkiewicz, Bull. Acad. Polon. Sci. Sér. Sci. Chim., 28 (1980) 297.
18 A. Isalgue, J. Ortin, V. Torra and J. Viñals, An. Fis., 76 (1980) 192.
19 J. Navarro, E. Cesari, V. Torra, J.-L. Macqueron, J.-P. Dubès and H. Tachoire, Thermochim. Acta, 52 (1982) 175.

20 V. Torra and H. Tachoire, J. Thermal Anal., 52 (1998) 663.
21 H. Tachoire and V. Torra, Thermochim. Acta, 110 (1987) 171.
22 F. Socorro, M. Rodríguez de Rivera and Ch. Jesus, J. Therm. Anal. Cal., 64 (2001) 357.
23 Discussion between Mrs. Chemtob, Tachoire and Calvet in Microcalorimétrie et Thermogenèse, no. 156, Éditions du Centre National de la Recherche Scientifique, Paris 1967, p. 329.
24 J. E. Callanan, J. Thermal Anal., 45 (1995) 359.
25 F. Socorro and M. Rodríguez de Rivera, J. Thermal Anal., 52 (1998) 729.
26 L. Alvarez, F. Socorro, I. de la Nuez and M. Rodriguez de Rivera, Thermochim. Acta, 344 (2000) 61.
27 F. Socorro and M. Rodríguez de Rivera, J. Therm. Anal. Cal., submitted.
28 R. H. Stokes, K. N. Marsh and R. P. Tomlins, J. Chem. Thermodyn., 1 (1969) 211.
29 K. N. Marsh and R. H. Stokes, J. Chem. Thermodyn., 1 (1969) 223.
30 B. Marongiu, I. Ferino and R. Monaci, J. Mol. Liquids, 28 (1984) 229.
31 J. Lerchner, G. Wolf, C. Auguet and V. Torra, Thermochim. Acta, (in preparation).
32 J. A. Dean Ed., 'Lange's Handbook of Chemistry', MacGraw-Hill 1985.
33 W. H. Press, S. A. Teukolsky, W. T. Vetterling and B. P. Flannery, Numerical Recipes in Fortran, Cambridge University Press 1992.